Near-barrier heavy-ion fusion: Role of boundary conditions in coupling of channels

P. W. Wen

Joint Institute for Nuclear Research, 141980 Dubna, Russia
and China Institute of Atomic Energy, 102413 Beijing, China

O. Chuluunbaatar

Joint Institute for Nuclear Research, 141980 Dubna, Russia
and Institute of Mathematics and Digital Technologies, Mongolian Academy of Sciences, 13330 Ulaanbaatar, Mongolia

A. A. Gusev

Joint Institute for Nuclear Research, 141980 Dubna, Russia

R. G. Nazmitdinov

Joint Institute for Nuclear Research, 141980 Dubna, Russia
and Dubna State University, 141982 Dubna, Russia

A. K. Nasirov

Joint Institute for Nuclear Research, 141980 Dubna, Russia
and Institute of Nuclear Physics, Ulugbek, 100214, Tashkent, Uzbekistan

S. I. Vinitsky

Joint Institute for Nuclear Research, 141980 Dubna, Russia
and Peoples' Friendship University of Russia (RUDN University), 117198 Moscow, Russia

C. J. Lin

China Institute of Atomic Energy, 102413 Beijing, China
and Department of Physics, Guangxi Normal University, 541004 Guilin, China

H. M. Jia

China Institute of Atomic Energy, 102413 Beijing, China

The problem of a quantum-mechanical description of a near-barrier fusion of heavy nuclei, that occurs at strong coupling of their relative motion to surface vibrations, is analyzed. To this end, an efficient finite-element method is proposed for numerically solving coupled Schrödinger equations with boundary conditions corresponding to total absorption. The method allows us to eliminate the instabilities in the numerical solutions that appear at a large number of coupled channels in some reactions. To illustrate the validity of our approach, the results of fusion cross section of the ^{64}Ni + ^{100}Mo and ^{36}S + ^{48}Ca reactions have been re-examined. The obtained results demonstrate a remarkable agreement with the available experimental data. It is found that experimental data can be reproduced with the use of the Woods-Saxon potential, without introducing the repulsive cores. It appears that the fusion cross sections at deep sub-barrier energies are sensitive to the potential pocket profile.

I. INTRODUCTION

Nuclear fusion phenomena have attracted considerable theoretical and experimental attention over several decades [1–7]. Although basic notions of this phenomenon are relatively well understood, there are still many hidden details that require clarification. This is especially important, for example, in light of synthesis of superheavy nuclei and evaluation of boundaries of the nuclear drip line. According to general wisdom, the latest problems are closely related to intimate knowledge of various stages of astrophysical nucleogenesis, from the Big Bang to creation of life on our Earth.

Thanks to significant improvement of experimental sensitivity in view of the remarkable development of semiconductor detectors and computational capability, it becomes

possible to systematically investigate stable and exotic nuclei at energies well below the Coulomb barrier. In particular, the fusion experimental data at deep sub-barrier energy have been measured down to 10^{-5} mb [8]. Evidently, already available experimental data require reliable qualitative and quantitative interpretation. For example, the threshold anomaly problem [9–11], diffuseness parameter anomaly problem [12,13], deep sub-barrier fusion hindrance and its associated impact on stellar evolution [14–16], subbarrier positive Q-value fusion enhancement [17–22], and above barrier fusion suppression phenomena, to name just a few, are challenges to the theory. It is at once apparent that the degree of accuracy of theoretical calculations may lead to different conclusions on the same phenomenon [8,23–29].

The cross sections of near–barrier and especially sub-barrier fusion of nuclei can be described within the coupled-channels models that are based on various approximations (e.g., Refs. [30–33]). In particular, the approach of directly constructing a numerical solution to the set of coupled Schrödinger equations (see for details Refs. [6,34]) provides a convenient ground from which to calculate the fusion cross sections. Note that colliding nuclei may develop large dynamical deformations. Consequently, this problem requires the consideration of large number of coupled channels (see, e.g., for discussion Refs. [35–37]). As a result, one needs to preserve the numerical accuracy of the calculations, and this requires carefully treating boundary conditions.

There are generally two approaches to construct the fusion cross sections based on the solving of the coupled-channels equations. The first one is to use the regular boundary condition and the complex potential [5]. The fusion is defined as the absorption of the incident flux due to the imaginary part of the potential. The fusion cross section can be predicted accurately by the explicit integration of the imaginary potential over the radial wave functions. The other approach adopts the incoming wave boundary condition (IWBC). It assumes that there is a strong absorption in the inner region such that the incoming flux never returns. In this case, it is enough to consider the real potential only [6]. Following the same theoretical ideas as in Ref. [6], we develop a new algorithm for solving a set of second-order differential equations. We consider the boundary conditions with a strict requirement of a complete absence of the reflected waves from the intrinsic region behind the barrier. We calculate the matrix elements of the interaction between colliding nuclei explicitly.

The structure of the paper is the following. The theoretical framework is briefly discussed in Sec. II. Results of numerical calculations on two fusion reaction systems within our approach are presented in Sec. III. A summary of our work is given in Sec. IV.

II. THEORETICAL FRAMEWORK

In this section, for the sake of completeness, we review the basic notions of the coupled-channels model (see for details, e.g., Refs. [6,30,34–36,38]).

A. Basic equations

The fusion cross sections, decomposed over partial waves, have the following form:

$$\sigma_f(E) = \frac{\pi \hbar^2}{2\mu E} \sum_{l=0}^{\infty} (2l + 1) P_l(E). \tag{1}$$

Here, E is the center-of-mass energy, $\mu = A_P A_T / (A_P + A_T)$ is the reduced mass, $A_{P(T)}$ is the mass of the projectile (target) nucleus, l is the orbital angular momentum, and $P_l(E)$ is the barrier penetration probability. Our task is to find the coefficients $P_l(E)$.

Consider a collision between two nuclei, taking into account the coupling of the relative motion between the centers of mass of the colliding nuclei, $\mathbf{r} = (r, \hat{\mathbf{r}})$ to a nuclear intrinsic motion ξ. The system Hamiltonian has the following form:

$$H(\mathbf{r}, \xi) = -\frac{\hbar^2}{2\mu} \nabla_{\mathbf{r}}^2 + V(\mathbf{r}) + H_0(\xi) + V_{\text{coup}}(\mathbf{r}, \xi), \tag{2}$$

where $H_0(\xi)$ describes the intrinsic structure, while the term $V_{\text{coup}}(\mathbf{r}, \xi)$ describes the coupling between the relative motion and the intrinsic structure. Note that the intrinsic degree of freedom ξ may have a finite spin I. In this case, for a fixed total angular momentum J and its z component M of the system, the channel wave function can be chosen in the following form:

$$\langle \hat{\mathbf{r}} \xi | (\alpha l I) J M \rangle = \sum_{m_l, m_I} \langle l m_l I m_I | J M \rangle Y_{l m_l}(\hat{\mathbf{r}}) \varphi_{\alpha I m_I}(\xi), \tag{3}$$

where $Y_{l m_l}(\hat{\mathbf{r}})$ is the spherical harmonics. The wave functions of the internal motion $\varphi_{\alpha I m_I}(\xi)$ is subject to the equation

$$H_0(\xi) \varphi_{\alpha I m_I}(\xi) = \epsilon_{\alpha I} \varphi_{\alpha I m_I}(\xi), \tag{4}$$

where α stands for quantum numbers associated with the intrinsic motion and $\epsilon_{\alpha I}$ is the corresponding eigenenergy. Expanding the total wave function with the channel wave functions as

$$\Psi_J(\mathbf{r}, \xi) = \sum_{\alpha, l, I} \frac{u_{\alpha l I}^J(r)}{r} \langle \hat{\mathbf{r}} \xi | (\alpha l I) J M \rangle, \tag{5}$$

one obtains the coupled-channels equations for $u_{\alpha l I}^J(r)$

$$\left[-\frac{\hbar^2}{2\mu} \frac{d^2}{dr^2} + \frac{l(l+1)\hbar^2}{2\mu r^2} + V(r) - E + \epsilon_{\alpha, I} \right] u_{\alpha l I}^J(r)$$
$$+ \sum_{\alpha', l', I'} V_{\alpha l I; \alpha' l' I'}^J(r) u_{\alpha' l' I'}^J(r) = 0, \tag{6}$$

where the coupling matrix elements $V_{\alpha, l, I; \alpha', l', I'}^J(r)$ are given as

$$V_{\alpha, l, I; \alpha', l', I'}^J(r) = \langle (\alpha l I) J M | V_{\text{coup}}(\vec{r}, \xi) | (\alpha' l' I') J M \rangle. \tag{7}$$

In solving the quantum problem in question, we employ the so-called isocentrifugal approximation (see details in Ref. [6]). In this approximation, the angular momentum of the relative motion in each channel is replaced by the total angular momentum. In this case, one ignores the change of the orbital angular momentum due to intrinsic excitations. Such approximation allows us to reduce several-fold the dimensionality of the set of differential equations that should be solved.

B. Vibrational coupling

To demonstrate all pros and cons of our approach we analyze couplings of the relative motion to surface vibrations of a target nucleus only, comparing our results with those well known from literature. Hereafter, for the sake of convenience, we consider the potential between the projectile and the target as a function of the relative distance r between them:

$$V(r) = V_{\mathcal{N}}(r) + V_C(r). \tag{8}$$

The potential contains the Coulomb term $V_C = Z_P Z_T e^2/r$ and a phenomenological nuclear potential $V_{\mathcal{N}}(r)$, that is chosen in the Woods-Saxon form:

$$V_{\mathcal{N}}(r) = -\frac{V_0}{1 + \exp[(r - R_0)/a_0]}. \tag{9}$$

Here, the parameters V_0, R_0, a_0 are the potential depth, potential radius, and diffuseness, respectively.

The nuclear coupling term of the Hamiltonian (2) can be generated by changing the target radius in the potential to a dynamical operator $R_0 + \hat{O}$ [39]. The surface operator $\hat{O}$ is defined as

$$\hat{O} = \frac{\beta_\lambda}{\sqrt{4\pi}} r_{\mathrm{coup}} A_T^{1/3} (a_{\lambda 0}^\dagger + a_{\lambda 0}), \tag{10}$$

where $a_{\lambda 0}^\dagger$ ($a_{\lambda 0}$) is the creation (annihilation) operator of the vibrational mode of the multipolarity λ. In this representation, the matrix element of the operator $\hat{O}$ has the following form:

$$\hat{O}_{nm} = \frac{\beta_\lambda}{\sqrt{4\pi}} r_{\mathrm{coup}} A_T^{1/3} (\sqrt{m}\,\delta_{n,m-1} + \sqrt{n}\,\delta_{n,m+1}), \tag{11}$$

where the n-phonon state of the multipolarity λ is defined as

$$|n\rangle = \frac{1}{\sqrt{n!}} (a_{\lambda 0}^\dagger)^n |0\rangle.$$

The deformation parameter β_λ, that defines the amplitude of the zero-point motion, can be determined from the experimental transition probability

$$\beta_\lambda = \frac{4\pi}{3 Z_T R_T^\lambda} \sqrt{\frac{B(E\lambda) \uparrow}{e^2}}, \tag{12}$$

where R_T^λ is the radius of the spherical nucleus. In our consideration, the variable r_{coup} is a free parameter, being slightly varied around the mean value 1.2 fm. The nuclear coupling matrix elements are then determined as

$$V_{nm}^{(\mathcal{N})}(r) = \langle n|V_{\mathcal{N}}(r, \hat{O})|m\rangle - V_{\mathcal{N}}^{(0)}(r)\delta_{n,m}, \tag{13}$$

where $V_{\mathcal{N}}(r, \hat{O}) \Longleftrightarrow V_{\mathcal{N}}(r, R_0 + \hat{O})$, $V_{\mathcal{N}}^{(0)}(r) \equiv V_{\mathcal{N}}(r)$ (see Eqs. (3.52)–(3.59) in Ref. [6] for more details). The latter term in Eq. (13) is introduced to counteract the coupling interaction in the entrance channel [40].

Thus, in the isocentrifugal approximation, the coupled-channels Schrödinger equation has the following form:

$$\left[-\frac{\hbar^2}{2\mu} \frac{d^2}{dr^2} + \frac{l(l+1)\hbar^2}{2\mu r^2} + V_{\mathcal{N}}^{(0)}(r) + \frac{Z_P Z_T e^2}{r} + \epsilon_n - E \right] \psi_{nn_o}$$

$$+ \sum_{n'=1}^{N} V_{nn'}(r) \psi_{n'n_o}(r) = 0. \tag{14}$$

In the above equation, ϵ_n is the excitation energy of the nth channel or threshold energy, $n = 1, ..., N$, that is defined by Eq. (4). The number n_o is a number of the open entrance channel with a positive relative energy $E_{n_o} = E - \epsilon_{n_o} > 0$, $n_o = 1, ..., N_o \leqslant N$, and the wave functions $\{\psi_{nn_o}(r)\}_{n=1}^{N}$ are components of a desirable matrix solution. The coupling matrix elements (7) are transformed to the matrix element $V_{nm}(r)$ that consists of the Coulomb and the nuclear potentials $V_{\mathcal{N}}^{(0)}(r)$ in each entrance channel.

The solution of Eq. (14) is obtained under the IWBC. Namely, it is assumed that there is a strong absorption inside the potential pocket. The asymptotic boundary conditions of such type are determined conventionally for components of matrix solutions $\{\psi_{nn_o}(r)\}_{n=1}^{N}$ in the open entrance channels n_o with a positive relative energy E_{n_o} by the following relations:

$$\psi_{nn_o}^{as}(r) = \begin{cases} \exp(-ik_n(r_{\min})r)T_{nn_o}, & r \leqslant r_{\min}, \quad k_n(r_{\min}) > 0, \\ H_l^-(k_n r)\delta_{n,n_o} - H_l^+(k_n r)R_{nn_o}, & r > r_{\max}. \end{cases} \tag{15}$$

The functions $H_l^\pm(k_n r) = \pm i F_l(\eta_n, k_n r) + G_l(\eta_n, k_n r)$ are the outgoing and the incoming Coulomb partial wave functions, respectively. They are determined by means of the regular $F_l(\eta_n, k_n r)$ and the irregular $G_l(\eta_n, k_n r)$ Coulomb partial wave functions [41]. Here, $k_n(r)$ is the local wave number for the nth channel

$$k_n(r) = \sqrt{\frac{2\mu}{\hbar^2}\left[E - \epsilon_n - \frac{l(l+1)\hbar^2}{2\mu r^2} - V_{\mathcal{N}}^{(0)}(r) - \frac{Z_P Z_T e^2}{r} - V_{nn}(r) \right]} \tag{16}$$

that depends on the excitation energy ϵ_n of the nth channel. The asymptotic behaviors of the functions $H_l^\pm(k_n r)$ are defined as

$$H_l^\pm(k_n r) \to \exp\left[\pm i\left(k_n r - \eta_n \ln(2k_n r) + \sigma_{ln} - \frac{l\pi}{2} \right) \right], \tag{17}$$

where $\eta_n = k_n Z_T Z_P e^2/(2E_n)$ is the Sommerfeld parameter; $\sigma_{ln} = \arg \Gamma(l + 1 + i\eta_n)$ is the Coulomb phase shift in open channels at $k_n = \sqrt{2\mu(E - \epsilon_n)}/\hbar > 0$.

On the other hand, for the components of $\psi_{nn_o}^{as}(r)$ with elements $n = N_o + 1, ..., N$, where n is restricted by the condition $E_n = E - \epsilon_n \leqslant 0$, we have

$$\psi_{nn_o}^{as}(r) = \begin{cases} \exp(|k_n(r_{\min})|r), & r \leqslant r_{\min}, \\ 0, & r \geqslant r_{\max}. \end{cases} \tag{18}$$

The conventional partial fusion probability $P_l(E)$ for the incident channel n_0 is determined by summation over all open

channels of intrinsic states at $k_n(r_{\min}) > 0$ for $n = 1, \ldots, N_o$:

$$P_l(E) \equiv T_{n_o n_o}^{(l)}(E) = \sum_{n=1}^{N_o} \frac{k_n(r_{\min})}{k_{n_o}} |T_{n n_o}|^2, \qquad (19)$$

where the incident wave number $k_{n_o} = \sqrt{2\mu(E - \epsilon_{n_o})/\hbar^2}$. Finally, the total fusion cross section is expressed as a sum over partial waves at the center of mass energy E, which is

$$\sigma_f(E) = \sum_{l=0}^{L} \sigma_f^{(l)}(E) = \frac{\pi}{k_{n_o}^2} \sum_{l=0}^{L} (2l+1) P_l(E). \qquad (20)$$

C. Boundary conditions

Prior to proceeding to the numerical analysis, a few comments are in order. In Eq. (15), $r_{\max}$ is set as a large enough distance where the interaction is weak, and the off-diagonal elements of the coupled matrix tend to be zero. The minimal point $r_{\min}$ is taken as the minimum of the potential pocket. The plane wave boundary condition at the left boundary $r_{\min}$ involves only the diagonal part of the coupling matrix element $k_n(r_{\min})$ from Eq. (16). This requires that the off-diagonal matrix elements tend to be zero. However, at $r_{\min}$, the distance between two nuclei is so short that the off-diagonal matrix elements are usually not zero. As addressed in Ref. [35], there can be sudden noncontinuous changes in the left boundary, and this will cause the distortion for the total wave function in the barrier region. To resolve this problem, we further develop the approach proposed in a series of papers [37,42–48].

First, it is reasonable to assume that at $r_{\max}$ the contribution of closed channels is negligible small. Consequently, we can use the conventional Dirichlet boundary condition at $r_{\max}$ for components of matrix solutions $\psi_{n n_o}(r_{\max}) = 0$ of Eq. (14) for $[n = 1, \ldots, N; n_o = N_o + 1, \ldots, N]$ in closed channels [see also Eq. (18)]. Second, at the left boundary we adopt the linear transformation method [37]. The essence of this method is the following:

Let consider the matrix $\mathbf{W}$ to be a symmetric matrix of our problem [see Eq. (14)] of the dimension $N \times N$

$$\begin{aligned} W_{nm} &= W_{mn} \\ &= \frac{2\mu}{\hbar^2} \left[\left(\frac{l(l+1)\hbar^2}{2\mu r^2} + V_{\mathcal{N}}^{(0)}(r) \right. \right. \\ &\quad \left. \left. + \frac{Z_P Z_T e^2}{r} + \epsilon_n \right) \delta_{nm} + V_{nm}(r) \right], \qquad (21) \end{aligned}$$

and the constant matrix in the vicinity of the left boundary point $r = r_{\min}$. In the above equation, $V_{nm}(r) = V_{nm}^{(N)}(r) + V_{nm}^{(C)}(r)$, where $V_{nm}^{(N)}(r)$ is obtained by Eq. (13) and $V_{nm}^{(C)}(r)$ is the Coulomb coupling matrix elements (see Eq. (28) in

Ref. [34] for more details). Here, the matrices $\mathbf{A}$ and $\tilde{\mathbf{W}}$ are the matrix of eigenvectors and the diagonal matrix of eigenvalues of the eigenvalue problem, respectively. Namely, we have

$$\mathbf{W A} = \mathbf{A} \tilde{\mathbf{W}}, \quad \{\tilde{\mathbf{W}}\}_{nm} = \delta_{nm} \tilde{W}_{mm},$$
$$\tilde{W}_{11} \leqslant \tilde{W}_{22} \leqslant \cdots \leqslant \tilde{W}_{NN}. \qquad (22)$$

In this case, the linear independent matrix solution $\{\phi_{nm}(r)\}_{n,m=1}^{N}$ of Eq. (14) can be written in the form

$$\phi_{nm}(r) = A_{nm} y_m(r), \qquad (23)$$

where functions $y_m(r)$ are solutions of the uncoupled equations

$$y_m''(r) + K_m^2 y_m(r) = 0, \quad K_m^2 = \frac{2\mu}{\hbar^2} E - \tilde{W}_{mm}. \qquad (24)$$

In open channels at $K_m^2 > 0$, $m = 1, \ldots, M_o \leqslant N$, the solutions $y_m(r)$ have the form

$$y_m(r) = \frac{\exp(-iK_m r)}{\sqrt{K_m}}, \qquad (25)$$

while in closed channels at $K_m^2 \leqslant 0$, $m = M_o + 1, \ldots, N$,

$$y_m(r) = \frac{\exp(|K_m| r)}{\sqrt{|K_m|}}. \qquad (26)$$

In this case, $\psi_{n n_o}(r)$ is expressed by the linear combinations of the linear independent solutions $\phi_{nm}(r)$

$$\psi_{n n_o}(r) = \sum_{m=1}^{M_o} \phi_{nm}(r) \hat{T}_{m n_o} \equiv \sum_{m=1}^{M_o} A_{nm} y_m(r) \hat{T}_{m n_o},$$
$$r = r_{\min}. \qquad (27)$$

In this way, the off-diagonal matrix elements have been considered in our calculations (see Sec. III). We consider the following boundary conditions in two endpoints. At $r = r_{\min}$, we have in terms of corresponding solutions A_{nm} $n, m = 1, \ldots, N$ at $K_m \geqslant 0$, $m = 1, \ldots, M_o \leqslant N$ for open exit channels and pure imagine $K_m < 0$, $m = M_o + 1, \ldots, N$ for closed exit channels

$$\begin{aligned} \psi_{n n_o}^{as}(r) &= \sum_{m=1}^{M_o} A_{nm} \frac{\exp(-iK_m r)}{\sqrt{K_m}} \hat{T}_{m n_o} \\ &\quad + \sum_{m=M_o+1}^{N} A_{nm} \frac{\exp(|K_m| r)}{\sqrt{|K_m|}} \hat{T}_{m n_o}^c, \quad r = r_{\min}. \quad (28) \end{aligned}$$

At $r = r_{\max}$, the asymptotic solutions are given in the terms of normalized Coulomb functions $\hat{H}_l^{\pm}(k_n r) = H_l^{\pm}(k_n r)/\sqrt{k_n}$, $k_n \geqslant 0$, $n = 1, \ldots, N_o \leqslant N$, and for components of $\psi_{n n_o}^{as}(r_{\max}) = o(1)$ with elements $n = N_o + 1, \ldots, N$ for closed channels,

$$\psi_{n n_o}^{as}(r) = \begin{cases} \hat{H}_l^-(k_n r) \delta_{n, n_o} - \hat{H}_l^+(k_n r) \hat{R}_{n n_o}, & r = r_{\max}, \\ 2|k_n|^{1/2} r^{l+1} \exp(-|k_n| r) U(l + 1 + \eta_n, 2l + 2, 2|k_n| r), & r = r_{\max}. \end{cases} \qquad (29)$$

Here $U(l + 1 + \eta_n, 2l + 2, 2|k_n| r)$ is Whittaker function [41], $\hat{T}_{n n_o}$ and $\hat{R}_{n n_o}$ are desirable partial transmission and reflection

amplitudes, and they are at $n_o = 1$ desirable—from a ground state $|i_o\rangle = |n_o - 1\rangle = |0\rangle$ of the intrinsic motion before the

collision, $\hat{T}^c_{mn_o}$ are transmission amplitudes in closed channels $m = M_o + 1, ..., N$.

The third type or Robin boundary conditions for solutions $\psi_{nn_o}(r)$ of Eq. (14) follow from their asymptotic expansion $\psi_{nn_o}(r)$

$$\left(\frac{d\psi_{nn_o}(r)}{dr} - \sum_{n'=1}^{N} G_{nn'}(r)\psi_{n'n_o}(r) \right)_{r=r_{\min}, r_{\max}} = 0, \quad (30)$$

where $G_{nn'}(r)$ are solutions of algebraic problem

$$\left(\frac{d\psi^{as}_{nn_o}(r)}{dr} - \sum_{n'=1}^{N} G_{nn'}(r)\psi^{as}_{n'n_o}(r) \right)_{r=r_{\min}, r_{\max}} = 0. \quad (31)$$

In this case, at fixed orbital momentum l the partial fusion probability

$$P_l(E) \equiv T^{(l)}_{n_o n_o}(E) \quad (32)$$

is given by summation over all possible intrinsic states:

$$
\begin{aligned}
T^{(l)}_{n_o n_o}(E) &= \sum_{m=1}^{M_o} \left| \hat{T}_{mn_o} \right|^2, \\
R^{(l)}_{n_o n_o}(E) &= \sum_{n=1}^{N_o} \left| \hat{R}_{nn_o} \right|^2, \\
T^{(l)}_{n_o n_o}(E) &= 1 - R^{(l)}_{n_o n_o}(E),
\end{aligned}
\quad (33)
$$

that we used $P^{(l)}_{n_o n_o}(E) \equiv T^{(l)}_{n_o n_o}(E)$ in the conventional formula for total fusion cross section (20). The above discussed ideas have been transformed to the improved version of the program KANTBP used in our calculations. This program is based on the finite-element method and will be presented in the forthcoming paper.

It is noteworthy that the condition $T^{(l)}_{n_o n_o}(E) + R^{(l)}_{n_o n_o}(E) - 1 = 0$ fulfills in below calculations with ten significant digits. This means that the calculated scattering **S** matrix is symmetric and unitary with an accuracy of the same order [45]. The reader can find details of the preceding version of the program KANTBP in Refs. [43,44].

III. RESULTS AND DISCUSSION

In order to validate our approach, we calculate the tunneling probability and fusion cross sections for ^{16}O + ^{144}Sm by means of KANTBP. We consider one incident channel and one coupled channel. Only the low-lying collective 3^- vibrational state of ^{144}Sm with the excitation energy 1.81 MeV is taken into account. Our results demonstrates a remarkable agreement with those obtained by the modified Numerov (MNumerov) method (employed in CCFULL) (see Fig. 1). The potential parameters, used in this calculation, produce a very steep potential pocket, with barrier height at 61.25 MeV and pocket minimum at 8.94 MeV. The lowest incident energy is 55 MeV, which is far higher than the potential minimum.

For most fusion reaction systems, the results predicted with the use of KANTBP and CCFULL are almost identical when there are few coupled channels at near-barrier incident energy. For example, we observe such the agreement as well
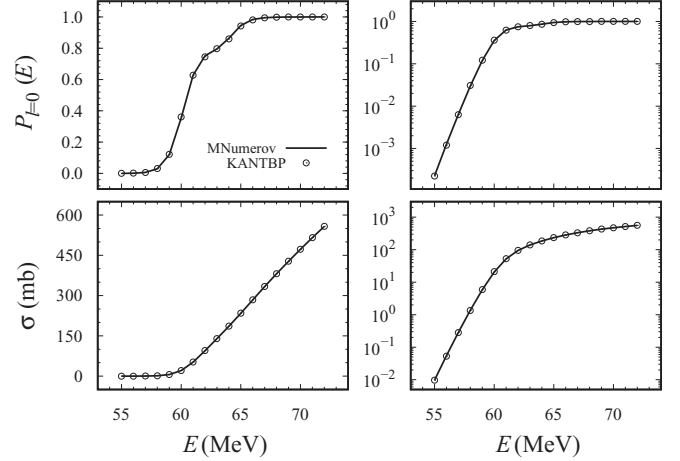
FIG. 1. The tunneling probability and fusion cross sections for ^{16}O + ^{144}Sm at linearization and logarithmic scale. The results obtained with the use of CCFULL are connected by solid line; also labeled as MNumerov. The results obtained by means of KANTBP are denoted by open circles. The parameters used in both calculations are taken from Ref. [34].

for ^{32}S, ^{40}Ca + ^{90,94,96}Zr reactions. The method introduced in these cases does not gain so much. However, when the number of coupled channels is increased considerably, the differences become more evident. Besides that, at the deep sub-barrier energy region, when the incident energy is close to the potential minimum, the fusion cross sections are very low and quite sensitive to the theoretical scheme.

In the following, we will consider ^{64}Ni + ^{100}Mo and ^{36}S + ^{48}Ca reactions and compare the results obtained by means of our approach and with the use of CCFULL. These two reactions have been both measured down to the deep sub-barrier energy region. Because of the instability of the modified Numerov method used in the CCFULL calculations, the shapes of the cross section lines can be different by connecting fusion cross section points at different incident energies. In order to avoid the shape uncertainty, we perform calculations at available experimental data except where there is no experimental point at the lowest energy.

In Table I, the adopted structure properties including excitation energies and deformation parameters for the nuclei used in this study are listed [49,50]. The low-lying collective 2^+ and 3^- vibrational states are considered. The radius parameter $r_{\rm coup}$ in the coupling interactions of Eq. (10) is assumed as

TABLE I. Adopted excitation energies E_x, spins and parities λ^π, $\pi = (-1)^\lambda$, and deformation parameters β_λ of the low-lying collective excited states for the indicated nuclei. The units of the excitation energies are in MeV.

Nucleus	^{36}S	^{48}Ca	^{64}Ni	^{100}Mo
E_{2^+} [49]	3.291	3.832	1.346	0.536
β_2 [49]	0.168	0.106	0.179	0.231
E_{3^-} [50]	4.193	4.507	3.560	1.908
β_3 [50]	0.376	0.230	0.201	0.218

1.2 fm for both target and projectile in all the following calculations. The numbers of target 3^- phonon, target 2^+ phonon, and projectile 2^+ phonon are denoted as $N_{T_{3^-}}$, $N_{T_{2^+}}$, and $N_{P_{2^+}}$ respectively. The total coupled-channels number will be $N_{\text{coup}} = (N_{T_{3^-}} + 1)(N_{T_{2^+}} + 1)(N_{P_{2^+}} + 1) - 1$ when all mutual excitations are included. It means that number of coupled equations in Eq. (14) is $N = N_{\text{coup}} + 1$.

The Woods-Saxon potential parameters in Eq. (9) derived from Akyüz-Winther (AW) parametrization [53,54] are used in the next step of calculations. This potential is obtained by means of fitting large-scale experimental scattering data, and has been successfully used in describing different kinds of reactions. It is written as

$$V_{\mathcal{N}}^{(0)}(r) = - \frac{V_0}{1 + \exp[(r - R_P - R_T)/a_0]}, \qquad (34)$$

where

$$V_0 = (16\pi\gamma a_0 \bar{R}) \text{ MeV},$$

$$\frac{1}{a_0} = 1.17\big[1 + 0.53\big(A_P^{-1/3} + A_T^{-1/3}\big)\big] \text{ fm}^{-1},$$

$$\bar{R} = \frac{R_P R_T}{R_P + R_T},$$

$$R_i = \big(1.2 A_i^{1/3} - 0.09\big) \text{ fm}, \quad i = P, T,$$

$$\gamma = 0.95\left(1 - 1.8\frac{(N_P - Z_P)(N_T - Z_T)}{A_P A_T}\right) \text{ MeV fm}^{-2}.$$

Here $N_{P(T)}$ is the neutron number of the projectile (target) nucleus. The fusion reaction $^{64}\text{Ni} + {}^{100}\text{Mo}$ had been measured at the superconducting linear accelerator ATLAS of Argonne National Laboratory [51]. The coupled-channel calculations that adopted different vibrational properties and nuclear radius were unable to reproduce the experimental fusion cross sections at deep sub-barrier energies. Hence, it was concluded that this system exhibits a hindrance for fusion. In Ref. [29], the CC calculations with the M3Y+ repulsion potential were used to describe the experimental data. Later, it was reported in Ref. [52] that the coupled-channel calculations, including a much deeper well potential than the standard AW potential [53,54] and a small radius parameter, will fit the experimental data well. In Ref. [19], the authors reproduced the major part of the experimental data by means of the coupled-channel method [35,36]. In these calculations, the standard AW potential, and the phonon numbers $N_{T_{3^-}} = 2$, $N_{T_{2^+}} = 2$, and $N_{P_{2^+}} = 2$, $N_{P_{3^-}} = 1$ are adopted. However, the slopes are deeper, and the predicted cross sections are generally smaller than the experimental data for energies $E \leqslant 125$ MeV.

The results obtained by means of KANTBP reproduce the experimental data well (see Fig. 2), without any special settings on the potential. In these calculations, 26 coupled channels are considered in the calculations, taking into account the number of excited states of the target: $N_{T_{3^-}} = 2$, $N_{T_{2^+}} = 2$, and $N_{P_{2^+}} = 2$. The detailed channels are listed in Table II. The standard AW potential [53,54] is adopted. Note that the above-barrier and below-barrier fusion cross sections are described within the experimental errors quite well. In contrast, the CCFULL results fluctuate when the incident energy $E < 130$ MeV, and far
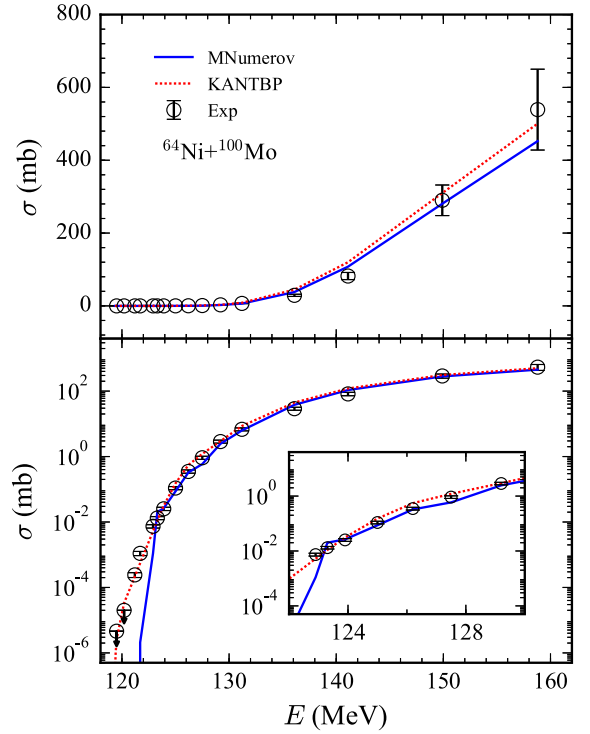
FIG. 2. Fusion cross sections for $^{64}\text{Ni} + {}^{100}\text{Mo}$. The experimental data (open circles) are from Ref. [51]. The fusion cross sections at the lowest two energies are the upper limits, which are indicated with arrows. The comparison of results obtained by means of CCFULL (solid line, also labeled as MNumerov), and by means of KANTBP (dotted line). All calculations are performed at the experimental incident energies except where there is no experimental point at the lowest energy. The insert is an enlargement of the sub-barrier fusion cross sections.

from the experimental data at deep sub-barrier energy region. We have also tested the predictions obtained with the use of CCFULL + stabilization method (see Ref. [55]), which is the same as the solid lines shown in Fig. 2. It should also be noted that when the Coulomb potential is changed to a spherical one, the instability at the low-energy tail will be shifted downward according to the radius parameters because the spherical Coulomb potential produces a deeper potential pocket and lower threshold energy.

In these calculations for $l = 0$, the largest diagonal matrix elements of the matrix $\hbar^2 \mathbf{W}/2\mu$ in Eq. (21) is 130.98 MeV. At the incident energy $E < 130.98$ MeV, the results of

TABLE II. The list of the 26 coupled channel for $N_{T_{3^-}} = 2$, $N_{T_{2^+}} = 2, N_{P_{2^+}} = 2$ in the form of $|T_{3^-} T_{2^+} P_{2^+}\rangle$ excluding the ground-state channel $|000\rangle$.

Configuration	Channels
Projectile	$|001\rangle, |002\rangle$
Target	$|100\rangle, |200\rangle, |010\rangle, |020\rangle, |110\rangle, |120\rangle, |210\rangle, |220\rangle$
Mutual	$|101\rangle, |201\rangle, |011\rangle, |021\rangle, |111\rangle, |121\rangle, |211\rangle, |221\rangle$
	$|102\rangle, |202\rangle, |012\rangle, |022\rangle, |112\rangle, |122\rangle, |212\rangle, |222\rangle$
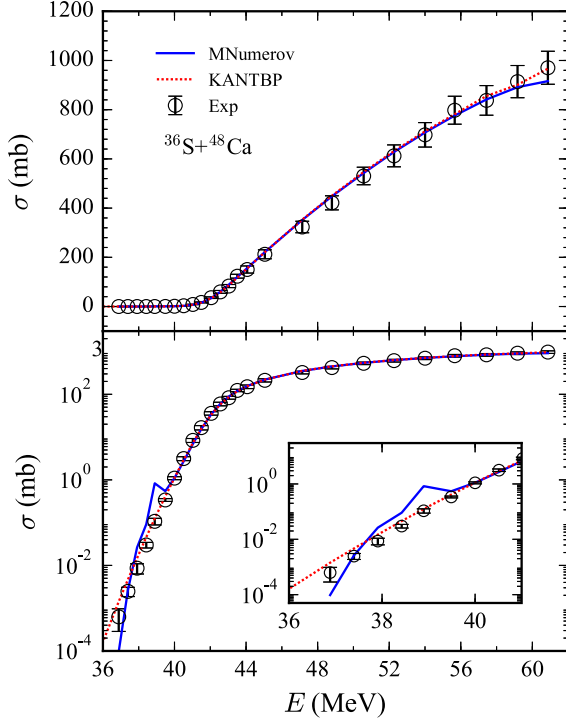
FIG. 3. Fusion cross sections for ^{36}S + ^{48}Ca. The notations are the same as in Fig. 2. The experimental data (open circles) on fusion cross sections are from Ref. [15]. The calculations are performed at the experimental incident energies except where there is no experimental point at the lowest energy. The insert is an enlargement of the sub-barrier fusion cross sections.

calculations should be influenced heavily by the nondiagonal elements. However, this effect is not considered in CCFULL. This observation explains the reason why the calculation start to fluctuate below this energy. The linear transform procedure introduced in this study changes not only the threshold energy by diagonalization, but also the number of open channels and closed channels. As a result, the final transmission matrix, and the cross sections will be affected. By considering the nondiagonal element in the **W** matrix at the left boundary, the calculation by KANTBP produces more stable results below about 130 MeV.

The fusion reaction ^{36}S + ^{48}Ca was performed at the accelerator of the Laboratori Nazionali di Legnaro of INFN [15]. A deep sub-barrier fusion hindrance feature of this reaction system had been reported. A large diffuseness parameter of $a = 0.95$ fm was used to reproduce the data above and below the barrier, which may actually mimic the presence of the deep inelastic reactions [12]. In Refs. [56] and [16], the double-folding ion-ion potential from different parametrization plus a repulsive contact term was adopted to describe the experimental cross sections. A weak and short-ranged imaginary potential is also used in Ref. [16] in order to remove some unwanted fluctuations in the theoretical calculation.

The results of fusion cross section calculations for ^{36}S + ^{48}Ca are presented in Fig. 3. In KANTBP, we use the same standard AW nuclear potential and the 26 coupled channels are considered, since there are the following excitations:

TABLE III. Woods-Saxon potential parameters V_0 (MeV), a_0 (fm), R_0 (fm), fitted at different combinations of the vibration phonon numbers $N_{T_{3^-}}$, $N_{P_{2^+}}$, $N_{T_{2^+}}$ for fusion excitation function of the ^{36}S + ^{48}Ca reaction. The standard AW-type potential parameters are listed in the second column for comparison.

	AW	Ch-0	Ch-1	Ch-17
$N_{T_{3^-}}$		0	0	1
$N_{T_{2^+}}$		0	0	2
$N_{P_{2^+}}$		0	1	2
V_0 (MeV)	61.338	72.325	61.355	55.911
a_0 (fm)	0.654	0.636	0.652	0.676
R_0 (fm)	8.143	8.272	8.298	8.167
V_B (MeV)	42.706	41.885	42.041	42.617
R_B (fm)	10.052	10.296	10.228	10.042
$\hbar\omega$ (MeV)	3.285	3.315	3.249	3.196

$N_{T_{3^-}} = 2$, $N_{T_{2^+}} = 2$, and $N_{P_{2^+}} = 2$. The results demonstrate good agreement with the experimental data near the barrier energy region. At the deep sub-barrier energy region, KANTBP results are slightly higher than the experiments, which may indicate the fusion hindrance feature for this reaction system. In contrast, CCFULL results manifest large fluctuations at the deep sub-barrier energy region. The reason of this fluctuation is the same as for the above discussed case (see Fig. 2). Namely, at $l = 0$ the largest diagonal matrix elements of the matrix $\hbar^2 \mathbf{W}/2\mu$ in Eq. (21) is 38.13 MeV. For the incident energy $E < 38.13$ MeV, there is a contribution of nondiagonal elements that are non-negligible. They are missing in CCFULL calculations.

Despite the many previous calculations mentioned above, it is of great interest to see whether the experimental fusion data can be explained by a simple Woods-Saxon-type potential model. In the following, we will try to find out that whether it is possible to describe well the experimental data by fitting the three parameters of the Woods-Saxon potential. The stability of the numerical method KANTBP is advantageous for fitting under some extreme parameters. The three Woods-Saxon potential parameters V_0, R_0, and a_0 are fitted to reproduce the fusion cross sections of ^{36}S + ^{48}Ca under different kinds of collective vibrations. The fitting parameters are shown in Table III, and the corresponding calculations under different conditions are given in Fig. 4. Different lines in the figure are denoted by the number of the coupled channels used. Three cases are examined here: 0, 1, and 17 coupled channels. The results of fitting demonstrate a good agreement with the experimental data for all three cases, in the above barrier energy region and below barrier energy region. The calculations under different collective vibrations are also almost overlapped.

The fitted Coulomb barrier properties, including barrier height V_B, barrier radius R_B, and the barrier curvature $\hbar\omega$, are listed in Table III. It can be seen that all fitted parameters in the last three columns are not very far from the stand AW parameters in the second column. It is not necessary to use very deep sub-barrier depths or very large diffuseness parameters to agree with the experimental data, like $V_0 = 165$ MeV and $a_0 = 0.95$ fm in previous study [15].
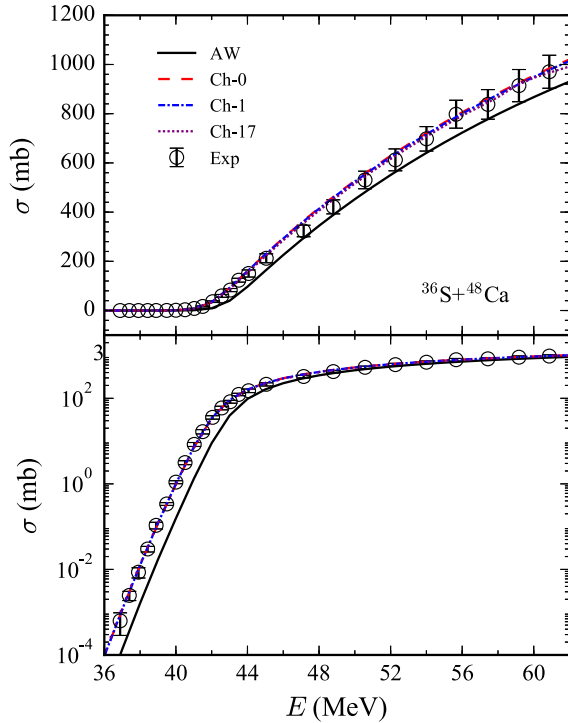
FIG. 4. Fusion cross sections for ^{36}S $+$ ^{48}Ca. The experimental data (open circles) on fusion cross sections are from Ref. [15]. The calculations with standard AW potential and 0 coupled channels are denoted by the solid lines. The fitted calculations performed with 0, 1, 17 coupled channels are represented by the dashed lines (Ch-0), dash-dotted lines (Ch-1), and dotted lines (Ch-17), respectively.

Corresponding fitted Woods-Saxon potentials are plotted in Fig. 5. The results obtained by the different methods show the different fitting the experimental data. However, the changing trends of the potential barrier can be seen from this figure. The fitted potentials reflect two tendencies in order to describe well the experimental fusion data theoretically, especially at the deep sub-barrier energy region. On the one hand, one can include fewer reaction channels and deeper potential inside the barrier pocket. On the other hand, one can make the
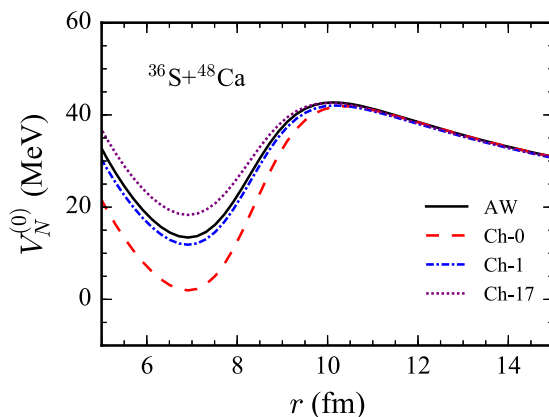
FIG. 5. The Woods-Saxon potentials calculated by different parameters listed in Table III. The notations are the same as in Fig. 4.

potential shallower and use more reaction channels. However, this reaction system can still be described well by using the simple Woods-Saxon potential. Comparing the lines AW and Ch-17, the Coulomb barriers are almost not changed, but the shapes of the potential well are quite different. This demonstrates that the deep sub-barrier fusion cross sections are very sensitive to the inner shape of the potential well, which have also been discussed in Ref. [25].

IV. SUMMARY

One of the standard methods to predict the fusion cross sections of light nuclei and capture cross section of the massive nuclei is to solve the set of coupled-channel differential equations with the use of the Numerov method. It is the heart of the full order coupling code CCFULL [34]. However, the CCFULL code, taking into account a large number of coupled channels, exhibits characteristics instabilities of the fusion excitation functions for some reactions. In the present paper, we developed a new algorithm for solving a set of second-order differential equations with the use of the finite-element method. To attack this problem, we further developed the approach proposed in series of papers [37,42–46,48]. Guided by our approach, we constructed the program KANTBP that was used for analysis of the fusion cross section of the ^{64}Ni $+$ ^{100}Mo and ^{36}S $+$ ^{48}Ca reactions. We demonstrated that our approach allows us to eliminate successfully the instabilities in the numerical solutions of the coupled-channels differential equations for these reactions.

In previous studies, special treatments of the potential, such as a large diffuseness parameter [15], a very deep potential plus a small radius parameter [52], or a repulsive core are needed to explain these experimental data related to the considered nuclei [16,29,56]. By means of our approach, we found that the fusion cross sections can be still described well with a simple Woods-Saxon-type potential. In particular, the fusion excitation function of the ^{64}Ni $+$ ^{100}Mo reaction is remarkably well described with the use of the standard AW potential. On the other hand, the fusion excitation function of the ^{36}S $+$ ^{48}Ca is described well by fitting of the Woods-Saxon potential parameters, without introducing the repulsive cores. It is demonstrated that the deep sub-barrier fusion cross sections are very sensitive to the potential pocket profile. The deep sub-barrier fusion cross sections can be used as a sensitive probe to explore the inner shape of the potential pockets.

[1] G. Montagnoli and A. M. Stefanini, Eur. Phys. J. A **53**, 169 (2017).

[2] B. B. Back, H. Esbensen, C. L. Jiang, and K. E. Rehm, Rev. Mod. Phys. **86**, 317 (2014).

[3] C. J. Lin, *Heavy-Ion Nuclear Reactions* (Harbin Engineering University Press, Harbin, 2015).

[4] J. J. Kolata, V. Guimarães, and E. F. Aguilera, Eur. Phys. J **52**, 123 (2016).

[5] L. F. Canto, P. R. S. Gomes, R. Donangelo, J. Lubian, and M. S. Hussein, Phys. Rep. **596**, 1 (2015).

[6] K. Hagino and N. Takigawa, Prog. Theor. Phys. **128**, 1061 (2012).

[7] N. Keeley, R. Raabe, N. Alamanos, and J. L. Sida, Prog. Part. Nucl. Phys. **59**, 579 (2007).

[8] M. Dasgupta, D. J. Hinde, A. Diaz-Torres, B. Bouriquet, C. I. Low, G. J. Milburn, and J. O. Newton, Phys. Rev. Lett. **99**, 192701 (2007).

[9] G. R. Satchler, Phys. Rep. **199**, 147 (1991).

[10] C. J. Lin, J. C. Xu, H. Q. Zhang, Z. H. Liu, F. Yang, and L. X. Lu, Phys. Rev. C **63**, 064606 (2001).

[11] L. Yang, C. J. Lin, H. M. Jia, D. X. Wang, N. R. Ma, L. J. Sun, F. Yang, X. X. Xu, Z. D. Wu, H. Q. Zhang, and Z. H. Liu, Phys. Rev. Lett. **119**, 042503 (2017).

[12] J. O. Newton, R. D. Butt, M. Dasgupta, D. J. Hinde, I. I. Gontchar, C. R. Morton, and K. Hagino, Phys. Rev. C **70**, 024605 (2004).

[13] J. O. Newton, R. D. Butt, M. Dasgupta, D. J. Hinde, I. Gontchar, C. R. Morton, and K. Hagino, Phys. Lett. B **586**, 219 (2004).

[14] C. L. Jiang, K. E. Rehm, R. V. F. Janssens, H. Esbensen, I. Ahmad, B. B. Back, P. Collon, C. N. Davids, J. P. Greene, D. J. Henderson, G. Mukherjee, R. C. Pardo, M. Paul, T. O. Pennington, D. Seweryniak, S. Sinha, and Z. Zhou, Phys. Rev. Lett. **93**, 012701 (2004).

[15] A. M. Stefanini, G. Montagnoli, R. Silvestri, S. Beghini, L. Corradi, S. Courtin, E. Fioretto, B. Guiot, F. Haas, D. Lebhertz, N. Mărginean, P. Mason, F. Scarlassara, R. N. Sagaidak, and S. Szilner, Phys. Rev. C **78**, 044607 (2008).

[16] G. Montagnoli, A. M. Stefanini, H. Esbensen, C. L. Jiang, L. Corradi, S. Courtin, E. Fioretto, A. Goasduff, J. Grebosz, F. Haas, M. Mazzocco, C. Michelagnoli, T. Mijatovic, D. Montanari, C. Parascandolo, K. E. Rehm, F. Scarlassara, S. Szilner, X. D. Tang, and C. A. Ur, Phys. Rev. C **87**, 014611 (2013).

[17] H. M. Jia, C. J. Lin, F. Yang, X. X. Xu, H. Q. Zhang, Z. H. Liu, L. Yang, S. T. Zhang, P. F. Bao, and L. J. Sun, Phys. Rev. C **86**, 044621 (2012).

[18] H. M. Jia, C. J. Lin, F. Yang, X. X. Xu, H. Q. Zhang, Z. H. Liu, Z. D. Wu, L. Yang, N. R. Ma, P. F. Bao, and L. J. Sun, Phys. Rev. C **89**, 064605 (2014).

[19] A. V. Karpov, V. A. Rachkov, and V. V. Samarin, Phys. Rev. C **92**, 064603 (2015).

[20] H. M. Jia, C. J. Lin, L. Yang, X. X. Xu, N. R. Ma, L. J. Sun, F. Yang, Z. D. Wu, H. Q. Zhang, Z. H. Liu, and D. X. Wang, Phys. Lett. B **755**, 43 (2016).

[21] P. W. Wen, Z. Q. Feng, C. Li, C. J. Lin, and F. S. Zhang, Chinese. Phys. Lett. **34**, 042501 (2017).

[22] P. W. Wen, Z. Q. Feng, C. Li, C. J. Lin, and F. S. Zhang, Chin. Phys. C **41**, 064102 (2017).

[23] C. J. Lin, Phys. Rev. Lett. **91**, 229201 (2003).

[24] K. Hagino, N. Rowley, and M. Dasgupta, Phys. Rev. C **67**, 054603 (2003).

[25] C. H. Dasso and G. Pollarolo, Phys. Rev. C **68**, 054604 (2003).

[26] C. J. Lin, Prog. Theor. Phys. Supp **154**, 184 (2004).

[27] Ş. Mişicu and H. Esbensen, Phys. Rev. Lett. **96**, 112701 (2006).

[28] T. Ichikawa, K. Hagino, and A. Iwamoto, Phys. Rev. Lett. **103**, 202701 (2009).

[29] Ş. Mişicu and H. Esbensen, Phys. Rev. C **75**, 034606 (2007).

[30] C. H. Dasso and S. Landowne, Comput. Phys. Commun. **46**, 187 (1987).

[31] J. Fernandez-Niello, C. H. Dasso, and S. Landowne, Comput. Phys. Commun. **54**, 409 (1989).

[32] M. Dasgupta, A. Navin, Y. K. Agarwal, C. V. K. Baba, H. C. Jain, M. L. Jhingan, and A. Roy, Nucl. Phys. A **539**, 351 (1992).

[33] J. O. Newton, C. R. Morton, M. Dasgupta, J. R. Leigh, J. C. Mein, D. J. Hinde, H. Timmers, and K. Hagino, Phys. Rev. C **64**, 064608 (2001).

[34] K. Hagino, N. Rowley, and A. T. Kruppa, Comput. Phys. Commun. **123**, 143 (1999).

[35] V. I. Zagrebaev, Prog. Theor. Phys. Supp **154**, 122 (2004).

[36] V. V. Samarin and V. I. Zagrebaev, Nucl. Phys. A **734**, E9 (2004).

[37] A. A. Gusev, O. Chuluunbaatar, S. I. Vinitsky, L. L. Hai, V. L. Derbov, and A. Góźdź, Bull. Peoples' Friendship Univ. Russia. Ser. Math. Inf. Sci. Phys. **3**, 38 (2016).

[38] T. Tamura, Rev. Mod. Phys. **37**, 679 (1965).

[39] A. Bohr and B. R. Mottelson, *Nuclear Structure* (Amsterdam, New York, 1974), Vol. II.

[40] K. Hagino, N. Takigawa, M. Dasgupta, D. J. Hinde, and J. R. Leigh, Phys. Rev. C **55**, 276 (1997).

[41] M. Abramowitz and I. A. Stegun, *Handbook of Mathematical Functions* (Dover, New York, 1965).

[42] O. Chuluunbaatar, A. A. Gusev, A. G. Abrashkevich, A. Amaya-Tapia, M. S. Kaschiev, S. Y. Larsen, and S. I. Vinitsky, Comput. Phys. Commun. **177**, 649 (2007).

[43] O. Chuluunbaatar, A. A. Gusev, V. P. Gerdt, V. A. Rostovtsev, S. I. Vinitsky, A. G. Abrashkevich, M. S. Kaschiev, and V. V. Serov, Comput. Phys. Commun. **178**, 301 (2008).

[44] A. A. Gusev, O. Chuluunbaatar, S. I. Vinitsky, and A. G. Abrashkevich, Comput. Phys. Commun. **185**, 3341 (2014).

[45] A. A. Gusev, O. Chuluunbaatar, S. I. Vinitsky, and A. G. Abrashkevich, Math. Mod. Geom. **3**, 22 (2015).

[46] A. A. Gusev, O. Chuluunbaatar, S. I. Vinitsky, A. G. Abrashkevich, A. Amaya-Tapia, M. S. Kaschiev, S. Y. Larsen, V. P. Gerdt, V. A. Rostovtsev, and V. V. Serov, https://www1.jinr.ru/programs/jinrlib/kantbp/indexe.html.

[47] A. A. Gusev, L. L. Hai, O. Chuluunbaatar, and S. I. Vinitsky, http://wwwinfo.jinr.ru/programs/jinrlib/kantbp4m.

[48] A. A. Gusev, S. I. Vinitsky, O. Chuluunbaatar, V. P. Gerdt, and V. A. Rostovtsev, Lect. Notes Comp. Sci. **6885**, 175 (2011).

[49] S. Raman, C. W. Nestor, and P. Tikkanen, Atom. Data. Nucl. Data. **78**, 1 (2001).

[50] T. Kibédi and R. H. Spear, Atom. Data. Nucl. Data. **80**, 35 (2002).

[51] C. L. Jiang, K. E. Rehm, H. Esbensen, R. V. F. Janssens, B. B. Back, C. N. Davids, J. P. Greene, D. J. Henderson, C. J. Lister, R. C. Pardo, T. Pennington, D. Peterson, D. Seweryniak, B.

Shumard, S. Sinha, X. D. Tang, I. Tanihata, S. Zhu, P. Collon, S. Kurtz, and M. Paul, Phys. Rev. C **71**, 044613 (2005).

[52] A. M. Stefanini, G. Montagnoli, F. Scarlassara, C. L. Jiang, H. Esbensen, E. Fioretto, L. Corradi, B. B. Back, C. M. Deibel, B. Di Giovine, J. P. Greene, H. D. Henderson, S. T. Marley, M. Notani, N. Patel, K. E. Rehm, D. Seweriynak, X. D. Tang, C. Ugalde, and S. Zhu, Eur. Phys. J. A **49**, 1 (2013).

[53] R. A. Broglia, R. A. Ricci, C. H. Dasso, and S. I. D. Fisica, *Nuclear Structure and Heavy-Ion Collisions: Varenna on Lake Como, Villa Monastero, 9th–21st July 1979* (North-Holland, Amsterdam, 1981).

[54] A. Winther, Nucl. Phys. A **594**, 203 (1995).

[55] N. R. K. Hagino and A. Kruppa, http://www.nucl.phys.tohoku.ac.jp/~hagino/ccfull.html.

[56] Ş. Mişicu and F. Carstoiu, Phys. Rev. C **83**, 054622 (2011).